

# Finite-Element Computational Fluid Dynamics Simulations Constrained by Phase-Contrast MRI Data

Giordano B. F. Borges<sup>1</sup>, Ivan R. Siqueira<sup>2</sup>, Joao L. A. Carvalho<sup>3</sup>, Jon-Fredrik Nielsen<sup>4</sup>, and Vinicius C. Rispoli<sup>5</sup>

<sup>1</sup>Department of Mathematics, University of Brasilia, Brasilia, Brazil, <sup>2</sup>Department of Mechanical Engineering, Pontifical Catholic University of Rio de Janeiro, Rio de Janeiro, Brazil, <sup>3</sup>Department of Electrical Engineering, University of Brasilia, Brasilia, Brazil, <sup>4</sup>Biomedical Engineering, University of Michigan, Ann Arbor, MI, United States, <sup>5</sup>UnB Gama College, University of Brasilia, Brasilia, Brazil

## Synopsis

Phase-contrast MRI (PC-MRI) data has been vastly used as boundary conditions in computational fluid dynamics (CFD) simulations. Recently, many authors also used measured flow data to enforce CFD solutions, based on the finite volume method (FVM). On the other hand, the finite element method (FEM) has notable advantages over FVM, such as higher order accuracy and more flexibility dealing with complex geometries. This work presents a finite-element implementation of a MRI-constrained CFD solver. This hybrid solver can be used to regularize PC-MRI data, providing solutions closer to the PC-MRI measurements than pure CFD. Feasibility of this approach is demonstrated using a modified 2D discretization of the Navier-Stokes and continuity equations, using FEM. In this demonstration, two velocity components were taken from a 4D PC-MRI dataset, and used to constrain the CFD solution over a 2D domain.

## Introduction

Phase-contrast MRI (PC-MRI) data have been used in the literature to perform MRI-constrained computational fluid dynamics (CFD) simulations using the finite volume method (FVM) with SIMPLER algorithm<sup>[1],[4]</sup>. However, the finite element method (FEM) is more flexible on dealing with complex geometries and boundary conditions, also allowing higher order approximations than FVM<sup>[5]</sup>. The aim of this work is to show that it is feasible to construct a more robust, hybrid MRI-CFD solver, based on FEM, that enforces PC-MRI measurements directly into the CFD routine. The hybrid solver can be used to regularize PC-MRI data, either reducing noise, or obtaining simulations that are closer to PC-MRI measurements than CFD alone. The feasibility of this approach is demonstrated using a modified 2D implementation of the Navier-Stokes-continuity equations, using the Garlekin FEM. In this demonstration, the CFD solution was constrained over a restricted 2D domain by two velocity components, taken from a 4D PC-MRI dataset.

## Methods

4DFT FGRE PC-MRI data were acquired from a flow phantom (Fig.1). PC imaging was performed on a 3T GE Discovery MR750 system (50mT/m, 200T/m/s), using a 32-channel head coil (resolution = 1.0×0.5×0.5mm<sup>3</sup>; FOV = 7.5×16×12cm<sup>3</sup>; Venc = 50cm/s; TR = 11.4ms; flip angle = 8.5°; temporal resolution = 91.2ms; scan time = 40 minutes; 9 NEX; pulse cycle 60bpm). The phantom's blood-mimicking fluid was modelled as a Newtonian and incompressible fluid. Hence, the steady incompressible 2D Navier-Stokes-continuity system of equations<sup>[6]</sup>,

$$\mathbf{u} \cdot \nabla \mathbf{u} = \nabla \cdot \boldsymbol{\sigma} \text{ and } \nabla \cdot \mathbf{u} = 0,$$

were discretized using FEM<sup>[5]</sup>, where  $Re$  is the Reynolds number<sup>[6]</sup>,  $\mathbf{u} = u_x \mathbf{i} + u_y \mathbf{j} \in \mathbb{R}^2$  is the velocity field,  $p$  is pressure, and  $\boldsymbol{\sigma} = -p\mathbf{I} + Re^{-1} [\nabla \mathbf{u} + \nabla \mathbf{u}^T]$  is the Newtonian stress tensor<sup>[6]</sup>. The discretization uses the residues functions given by the governing equations' weak form<sup>[5]</sup>,

$$R_m(\mathbf{u}, p) = \int_{\Omega} (\mathbf{u} \cdot \nabla \mathbf{u}) \cdot \boldsymbol{\psi} d\Omega + \int_{\Omega} \boldsymbol{\sigma} : \nabla \boldsymbol{\psi} d\Omega - \int_{\Gamma} (\mathbf{n} \cdot \boldsymbol{\sigma}) \cdot \boldsymbol{\psi} d\Gamma$$

and

$$R_c(\mathbf{u}) = \int_{\Omega} (\nabla \cdot \mathbf{u}) \phi d\Omega,$$

where  $\phi \in \mathbb{R}$ ,  $\boldsymbol{\psi} \in \mathbb{R}^2$  are weight functions. The discretized equations were written as a linear system  $\mathbf{J}\mathbf{c} = -\mathbf{R}^{[5]}$ , where  $\mathbf{J}$  is the Jacobian matrix of the residues,  $\mathbf{R}$  is the residues vector, and  $\mathbf{c}$  is the solution vector, containing velocity and pressure. To incorporate PC-MRI measurements into the CFD solver, the minimization

$$\min_{\mathbf{c}} \frac{1}{2} \|\mathbf{J}\mathbf{c} + \mathbf{R}\|_2^2 + \frac{\lambda}{2} \|\mathbf{S}\mathbf{c} - \mathbf{u}_{mri}\|_2^2$$

is performed using Newton's method, where  $\mathbf{S}$  is a matrix used to compare velocities on solution vector  $\mathbf{c}$  with the measured PC-MRI signal  $\mathbf{u}_{mri}$ , since these vectors may have different sizes. The lumen was manually outlined to define the computational mesh. Simulation grid was designed with 1.0×0.5mm<sup>2</sup> element resolution using Q2P<sub>1</sub> elements<sup>[5]</sup>. The Reynolds number for the problem was calculated as  $Re = 110$ . The PC-MRI velocity profile was set at the inlet of the flow domain together with no-slip boundary condition. MRI-constrained CFD solutions were obtained using two MRI-measured velocity components for different  $\lambda$ . A denoising experiment was performed, by adding 7.5cm/s standard deviation Gaussian noise to the measured PC-MRI data. Finally, the results were quantitatively and qualitatively compared with the "ground truth" 2D PC-MRI data\*.

## Results and Discussion

Figure 2 shows the  $u_x$  velocity component for: PC-MRI (Fig.2(a)), pure CFD solution,  $\lambda = 0$  (Fig.2(b)), and PC-constrained CFD solution,  $\lambda = 10^{-2}$  (Fig.2(c)). The constrained solution (Fig.2(c)) is closer to the measured PC-MRI data (Fig.2(a)) than pure CFD (Fig.2(b)). Moreover, this behavior is quantitatively confirmed using the signal-to-error ratio (SER), considering the measured PC-MRI as "ground truth" signal. While the pure CFD solution provided 4.53dB SER, the MRI-constrained CFD solution provided 8.17dB SER. This shows that constrained CFD solution can produce more realistic velocity fields. In Fig.2(b), there is a noticeable misbehavior of the solution in the center of the domain, near the bifurcation. For this problem's Reynolds number, the Navier-Stokes equation's diffusive term ( $\Delta^2 \mathbf{u}$ ) is much smaller than the convective term ( $\mathbf{u} \cdot \nabla \mathbf{u}$ ) causing amplification of solution errors. Then, this solver implementation requires numerical stabilization treatment<sup>[7]</sup>. Figure 3 shows the velocity fields from the denoising experiment for: PC-MRI (Fig.3(a)), noise corrupted PC-MRI, (Fig.3(b)) and CFD solution constrained by noisy PC-MRI,  $\lambda = 10^{-3}$  (Fig.3(c)). The constrained solution (Fig.3(c)) corrected the noisy PC flow (Fig.3(b)), leading to a solution that is very similar to original PC-MRI. This was quantitatively confirmed using the signal-to-noise ratio (SNR), considering PC-MRI as "ground truth" signal. The noisy PC-MRI has 5.39dB SNR, whereas the CFD solution constrained by noisy PC-MRI provided 6.86dB SNR. This 1.47dB SNR increase shows that MRI-constrained CFD can also be used for denoising PC-MRI velocity fields.

## Conclusions

This work shows that the proposed hybrid CFD-MRI finite-element solver is viable and can be used to obtain numerical solutions that are similar to the measured flow data, while satisfying the fluid physics equations; and also for reducing noise. In future works, a streamline-upwind stabilization term<sup>[7]</sup>, for high Reynolds number, will be implemented on a 3D steady version of this FEM based solver.

## Acknowledgements

Work supported by the 2015/2016 Institutional Scientific Initiation Program (PIBIC/UnB) from the University of Brasilia Research and Graduate Chamber (DPP/UnB).

## References

[1] Funamoto K, et al. ABE 37:1105, 2009. [2] Nielsen JF, et al. Proc ISMRM 17:3858, 2009. [3] Rispoli VC, et al. Proc ISMRM 22:2490, 2014. [4] Christodoulou AG, et al. Proc ISMRM 23:2735, 2015. [5] Gresho PM et al. Incompressible Flow and the Finite Element Method, 1998. [6] Chorin AJ, et al. A Mathematical Introduction to Fluid Mechanics, 2000. [7] Donea J et al. Finite Element Method for Flow Problems, 2003. \*MATLAB code available at: <http://bit.do/vrispoli>

## Figures



Figure 1. Carotid flow phantom (Phantoms by Design, Inc., Bothell, WA).

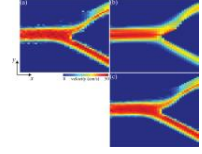


Figure 2. Velocity component on x direction: (a) measured PC-MRI data; (b) pure CFD solution ( $\lambda = 0$ ); and (c) CFD solution constrained by PC-MRI ( $\lambda = 10^{-2}$ ).

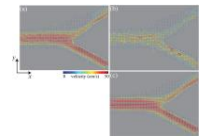


Figure 3. Vector field visualization: (a) measured PC-MRI data; (b) PC-MRI corrupted by Gaussian noise (standard deviation: 7.5cm/s); and (c) CFD solution constrained by noisy PC-MRI ( $\lambda = 10^{-2}$ ).